Drug Development and Industrial Pharmacy, 23(12), 1177–1189 (1997)

RESEARCH PAPER

Use of DSC to Study the Degradation Behavior of PLA and PLGA Microparticles

Gabriele Reich

Institute for Pharmaceutical Technology and Biopharmaceutics, Heidelberg University, Im Neuenheimer Feld 366, 69120 Heidelberg, Federal Republic of Germany

ABSTRACT

Poly(D,L-lactide) (PLA) and poly(D,L-lactide-co-glycolide) (PLGA) microparticles were evaluated for their in vitro degradation behavior in 0.1 M phosphate buffer pH 7.4 at 37°C. The influence of polymer characteristics, particle size, and preparation technique was investigated. Differential scanning calorimetry (DSC) was used to follow the time-dependent physical and morphological changes within the hydrated and dried microparticles, to determine the physical state of the absorbed water, and to detect penetration of buffer ions into the particle bulk. Results were compared with degradation kinetics obtained by gel permeation chromatography (GPC) and gravimetry. The latter revealed triphasic degradation profiles for R 202 and RG 755 microparticles with a mean particle size of 55 μm and 60 μm, respectively. An induction period was followed by a period of accelerated ester cleavage pre-onset of erosion and a final period of slow ester cleavage post-onset of erosion. According to DSC data the induction period is characterized by a glassy hydrated polymer matrix with a $T_{gH} > 37°C$. *The induction period* (t_i) *correlated well with the lag-time of* T_{gH} *to reach 37°C* ($t_{lag\ 37°C}$), *thus confirming the importance of chain mobility for the degradation kinetic. The final decrease in the rate of ester chain cleavage post-onset of erosion turned out to be the result of an increase in matrix permeability for buffer ions inducing sodium salt formation and phase separation of the water-soluble degradation products within the particle bulk. Particle size effects depended on the preparation technique. A decrease in the degradation rate with a decrease in mean particle size was only observed when the molecular weight distribution of the polymer was not affected by the prepa-*

ration procedure used to reduce the particle size. According to DSC data, the effect is due to a faster and more continuous release of the water-soluble degradation products from the smaller particles, thus reducing their plasticizing and autocatalytic effects within the particle bulk.

INTRODUCTION

The use of biodegradable polymers in controlling the release of drugs has become important in the formulation of pharmaceuticals. Due to their excellent biocompatibility and their FDA-approval for the preparation of controlled-release systems, biodegradable polymers based on poly(L-lactide) (PLLA), poly(D,L-lactide) (PLA), and poly(D,L-lactide-co-glycolide) (PLGA) often provide the basis for parenteral monolithic and particular devices (1–6). Because of their enormous potential in drug targeting (7) and their excellent compliance, particulate systems are usually favored over monolithic devices.

Interestingly, most of the work concerning PLLA, PLA, and PLGA degradation has been carried out with monolithic devices such as rods and disks (1,3,8–12). The results of these studies clearly reveal a 'heterogeneous bulk degradation pattern' of these large size devices leading to a surface/center differentiation with a faster degradation in the center part due to an autocatalytic effect of enclosed acidic degradation products. Although a core/shell differentiation has also been reported for microparticles in vitro (13) and in vivo (14,15), data obtained from large size devices cannot, however, be directly extrapolated to small size devices such as micro- and nanoparticles. Due to their huge specific surface, which probably allows a faster release of the acidic degradation products, it has generally been assumed that particulate systems degrade at a slower rate than macroscopic implants. In fact, a decrease in the overall degradation rate of microparticles with decreasing particle size has recently been demonstrated (16). The exact mechanism leading to this phenomenon is, however, not fully understood. Moreover, the kinetics of ester chain cleavage during the different stages of the degradation process are still a matter of debate. Mono- and biphasic degradation profiles of PLA and PLGA microparticles have been reported in the literature (5,6,17–19). However, a detailed understanding of the mechanisms underlying the different kinetics is not yet available. One major reason is that analytical techniques such as gel permeation chromatography (GPC), gravimetry, and scanning electron microscopy (SEM) cannot give any information on polymer/medium interactions and/or physical changes within the particle matrix occurring during hydration and degradation. In the present study, differential scanning calorimetry (DSC) was used to monitor the physical state of both the hydrated particle matrix and the absorbed water, to detect penetration of buffer ions into the particle bulk, and to determine morphological changes within the particles. Results were compared with kinetic degradation data obtained by GPC and gravimetry with the aim to mechanistically elucidate the complex degradation pattern of PLA and PLGA microparticles of various composition and particle size. Special attention was paid to the influence of the particle preparation technique, since it has recently been demonstrated that probe sonication during microsphere processing can lead to a tremendous degradation of PLA and PLGA polymers (20,21).

MATERIALS AND METHODS

Materials

Poly(D,L-lactide) (PLA; R 202: weight average molecular weight [M_W] = 14.5 kDa, polydispersity index [PD] = 1.3, T_g = 48.2°C) and poly(D,L-lactide-co-glycolide 75/25) (PLGA 75/25; RG 755: M_W = 66.8 kDa, PD = 1.7, T_g = 47.6°C) were obtained from Boehringer Ingelheim, Ingelheim, Germany. Hereafter, the polymers will be designated by their trade names: R 202 and RG 755. Polyvinylalcohol (PVA: M_W = 40 kDa; 88% hydrolyzed) was supplied by Hoechst AG, Frankfurt, Germany. All other chemicals and solvents were of analytical grade or better.

Preparation of Microparticles

R 202 and RG 755 microparticles with a mean particle size of 50–60 μm were prepared by a modified o/w emulsion evaporation process according to Cohen et al. (5). Briefly, the polymer (0.5 g) was dissolved in methylene chloride (2 ml). This solution was poured, under vigorous mixing using a magnetic bar, into 4 ml of an aqueous solution of PVA (1%, w/v) saturated with methylene chloride. The resulting o/w emulsion was

poured into 400 ml of a 0.1% PVA solution and continuously stirred for 3 hr at room temperature until most of the methylene chloride was evaporated. The resulting microparticles were centrifuged, washed three times with double-distilled water, and vacuum-dried into a powder.

Microparticles with a mean particle size of approximately 2 μm were prepared by two different techniques; a modified version of the aforementioned w/o emulsion solvent evaporation technique using probe sonication at 50 W for 30 sec instead of a magnetic bar to prepare the o/w emulsion, and a novel flocculation technique based on acetone as water-miscible organic solvent, thus avoiding probe sonication. In the flocculation technique (details concerning the mechanism of particle formation will be presented in a forthcoming paper), the polymer (0.5 g) was dissolved in acetone (10 ml). To this solution an isopropanol/water (1/1) mixture (20 ml) was poured under moderate stirring using a magnetic bar. The microparticles formed spontaneously due to a rapid diffusion of the acetone into the isopropanol/water mixture. After further dilution with double-distilled water (200 ml), the microparticles were collected by filtration and vacuum-dried.

The physicochemical characteristics of the microparticles prepared from different polymers and different techniques and the designations used hereafter are given in Table 1. Residual solvents were $<0.01\%$.

Degradation Studies

Microparticles (ca. 50 mg) were incubated with 20 ml of a 0.1 M phosphate buffer saline (PBS) pH 7.4 and stored at 37°C under moderate horizontal agitation. At predetermined time intervals, six samples of each series were collected. The microparticles were isolated from the buffer solution by filtration and washed two times with cold water. Three samples were directly analyzed for their glass transition temperature (T_{gH}), the physical state of the absorbed water, and penetration of buffer ions. The other three samples were vacuum-dried to constant weight and thereafter analyzed for molecular weight changes, mass loss, and physical and morphological changes. The buffer solutions were analyzed for pH changes.

Analytical Methods

Mean particle size and particle size distribution of the microparticles were measured by laser light scattering (Mastersizer X, Malvern, UK). Residual solvents were analyzed by headspace GC (HS 100, GC Sigma 2000, Perkin-Elmer, Überlingen, Germany).

The initial M_W and a PD (PD = M_W/M_n) of the polymer raw materials and microparticles and the corresponding changes upon immersion of microparticles of PBS pH 7.4 at 37°C were determined by gel permeation chromatography (GPC). Polymer samples dissolved in tetrahydrofuran (THF) to a final concentration of 5 mg/ml were filtered through a 0.45-μm filter before injection and eluted through two serially set 10 μm-PL-gel columns of 10^3 Å and 10^5 Å pore size (Polymer Laboratories, Shropshire, UK) at a flow rate of 1 ml/min and a temperature of 35°C (column oven from Knauer, Berlin, Germany). Calibration was carried out with monodisperse polystyrene standards (molecular weights between 1 kDa and 1400 kDa) from Merck, Darmstadt, Germany. The elution profiles were detected

Table 1

Preparation and Physicochemical Characteristics of PLA and PLGA Microparticles

Sample/no.	Polymer	Preparation Technique[a]	Mean Particle Size (μm)	M_w (kDa)[b]	PD[b]	Tg (°C)[c]
R 202/I	R 202	o/w-ESE; magnetic bar	55.0	14.4	1.3	47.9
RG 755/I	RG 755	o/w-ESE; magnetic bar	60.0	62.3	1.8	47.4
RG 755/II	RG 755	o/w-ESE; probe sonication	2.5	46.5	8.2	43.6[d]
RG 755/III	RG 755	Flocculation	1.8	63.5	1.7	48.0

[a]ESE: emulsion solvent evaporation.
[b]M_W, PD: determined by GPC, polystyrene standards.
[c]T_g: determined from the second heating cycle.
[d]First heating cycle evidenced one T_g.

refractometrically (differential refractometer type 198.00 from Knauer, Berlin, Germany) at 35°C. The data were analyzed by a GPC integrator from Shimadzu, Kyoto, Japan.

Mass loss of the microparticles was determined gravimetrically from the sample weight (w_o) before immersion in PBS pH 7.4 and the weight of the dried samples (w_t) after various incubation times in PBS pH 7.4 at 37°C according to the following equation:

$$\text{Mass loss } (\%) = 100\ (w_o - w_t)/w_o \quad (1)$$

The glass transition temperature (T_{gH}) of the hydrated samples, the physical state of the absorbed water, and the uptake of buffer ions into the particle bulk were analyzed by differential scanning calorimetry (DSC) using a DSC system TA 3000 from Mettler, Greifensee, Switzerland, equipped with a DSC 30 low-temperature cell and a TC 10A processing unit. Approximately 10 mg of each hydrated sample was accurately weighed into aluminum pans suitable for volatile compounds, hermetically sealed, and scanned under nitrogen atmosphere from -120°C to 200°C with a heating rate of 10°C/min. A covered, empty pan was used as reference. Calibration of the heat of fusion and the temperature scale was carried out with indium and indium, and lead and tin, respectively. T_{gH} was taken as the midpoint of the baseline shift associated with heat capacity (c_p) changes. The amount of bulk-like water was estimated from the melting enthalpy (ΔH_m) associated with the melting peak (T_m) of water around 0°C. Penetration of buffer ions into the particle bulk was detected by a shoulder prior to the main water melting peak (T_m) at 0°C or by a distinct shift of T_m to a temperature below 0°C.

DSC was also used to determine glass transition temperatures (T_{gD}) and other phase transitions of the dried samples indicating morphological changes within the particle matrix. For this purpose the dried samples were scanned two times from -120°C to 200°C at a heating rate of 20°C/min. Glass transition temperatures (T_{gH}) were again taken as the midpoints of the baseline shifts associated with c_p changes. Crystallization and/or other phase separation phenomena were recognized by the appearance of additional endothermic peaks or baseline shifts. Thermograms obtained from the first heating cycle provided information on the actual physical and morphological changes within the particle matrix. Phase transitions determined from the second run reflected equilibrium states.

Medium pH was followed potentiometrically with a pH-meter from Metrohm, Bernhausen, Germany.

RESULTS AND DISCUSSION

Degradation of R 202 Microparticles

The R 202/I microparticles prepared by the w/o emulsion solvent evaporation technique were spherical in shape with a mean particle size of 55 μm. The size distribution was relatively small with less than 5% having a diameter below 20 μm. As evidenced by the GPC data listed in Table 1, the preparation procedure was rather gentle and had no significant effect on the molecular weight distribution (M_w, PD) of the polymer. Due to the low residual solvent (<0.01%), the glass transition temperature was well above 37°C.

The log M_w versus time profiles of R 202/I microparticles immersed in 0.1 M PBS pH 7.4 of 37°C are given in Fig. 1. The graph clearly indicates a triphasic degradation profile. An initial induction period (t_i) of 44 days with a slow rate of hydrolysis ($k_i = 0.5 \times 10^{-3}\ d^{-1}$) was followed by an accelerated degradation phase ($k_1 = 1.1 \times 10^{-2}\ d^{-1}$) and a final slow down ($k_2 = 2.8 \times 10^{-3}\ d^{-1}$) at day 92, corresponding to $t_{lag\ k2}$. Mass loss analysis (see Table 2) revealed that the final degradation phase characterized by the rate constant k_2 started 12 days post-onset of accelerated bulk erosion.

To elucidate the mechanism underlying the three different degradation kinetics (k_i, k_1, k_2) and their respective duration (t_i, $t_{lag\ k2}$), a DSC study of the hydrated and dried samples was undertaken. First, it was important to consider the physical state of the hydrated microparticles, since water has been reported to act as

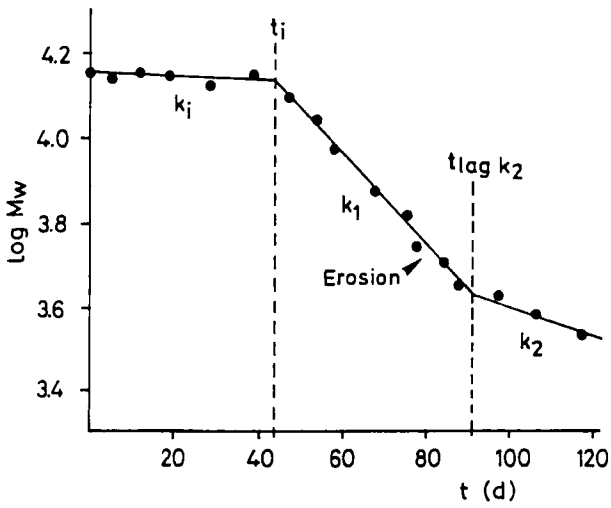

Figure 1. Time-dependent M_w-changes of R 202/I microparticles immersed in 0.1 M PBS pH 7.4 of 37°C (n = 3).

Table 2

In Vitro Degradation Kinetics of PLA and PLGA Microparticles in 0.1 M PBS pH 7.4 of 37°C (n = 3)

Sample/no.	t_i (d)[a]	$t_{lag\ k2}$(d)[b]	$t_{lag\ ML}$(d)[c]	$k_i \times 10^3$ (d^{-1})[d]	$k_1 \times 10^2$ (d^{-1})[d]	$k_2 \times 10^3$ (d^{-1})[d]
R 202/I	44	92	80	0.5	1.1	2.8
RG 755/I	33	84	76	4.5	1.8	3.3
RG 755/II	1	16	<1	—	4.2	2.9
RG 755/III	56	>120	nd[e]	2.4	1.4	nd[e]

[a] t_i: Duration of induction period.
[b] $t_{lag\ k2}$: Lag-time of terminal degradation phase post-onset of erosion.
[c] $t_{lag\ ML}$: Lag-time of accelerated mass loss.
[d] k_i, k_1, k_2: First-order rate constants of hydrolytic degradation during induction period, accelerated and terminal phase.
[e] nd: not determined.

a plasticizer, thereby decreasing the T_g. Thus, hydrated R 202/I microparticles after various days of incubation pre-onset of accelerated bulk erosion were subjected to a DSC scan from -120 to 200°C. Fig. 2 shows the DSC thermograms in the temperature range of the glass transitions; e.g., between 20°C and 60°C. Absolute T_{g0} and T_{gH} values are given in Tables 1 and 3. In fact, the T_{g0} of the polymer was gradually lowered upon hydration with a shift from 47.9°C down to 41.6°C and 41.1°C after 2 and 10 days of incubation, respectively. The lag-time ($t_{lag\ 37°C}$) of the glass transition (T_{gH}) to reach the incubation temperature of 37°C was found to be 45 days. From day 60, a second phase transition (T_{gH2}) appeared near 42°C and intensified as time progressed. Post-onset of accelerated mass loss, it was difficult to determine the first glass transition temperature (T_{gH1}), since it started to overlap with the melting peak associated with the accelerated uptake of bulk water (Fig. 3).

From the aforementioned DSC data it is obvious that the R 202/I microparticles remained in a glassy state

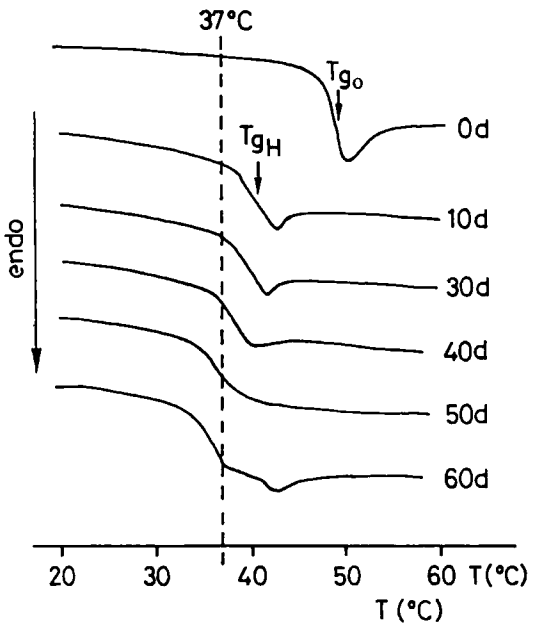

Figure 2. DSC thermograms of hydrated R 202/I microparticles after various incubation times in 0.1 M PBS pH 7.4 of 37°C.

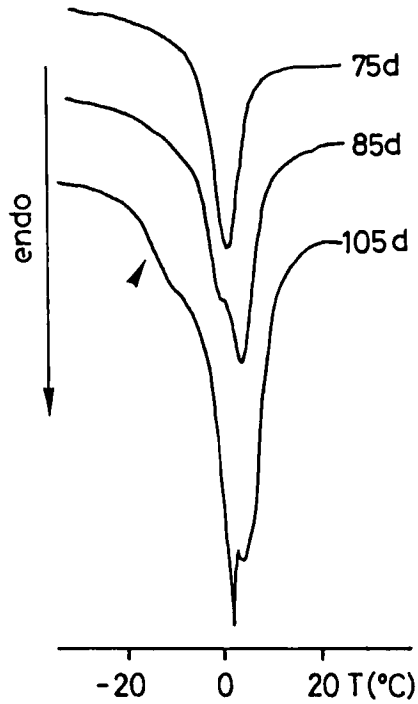

Figure 3. Melting endotherms of water within hydrated R 202/I microparticles pre-onset and post-onset of erosion.

Table 3

Thermal Characteristics of Hydrated PLA and PLGA Microparticles During In Vitro Degradation in 0.1 M PBS pH 7.4 of 37°C (n = 3)

Sample/no.	T_{gH} (°C)[a] 2 days	T_{gH} (°C)[a] 10 days	ΔT_{gH} (°C)[b] 2 days	ΔT_{gH} (°C)[b] 10 days	$t_{lag\ 37°C}$ (d)[c]
RG 202/I	41.6	41.1	2.2	2.3	45
RG 755/I	38.8	38.1	4.4	5.1	33
RG 755/II	30.4	38.4	6.2	2.3	<1
RG 755/III	39.9	39.4	2.1	1.9	57

[a] T_{gH}: Glass transition temperature of hydrated samples.
[b] $\Delta T_{gH} = T_{gHonset} - T_{gHend}$.
[c] $t_{lag\ 37°C}$: Lag-time of $T_{gH} \leq 37°C$.

with restricted chain mobility for more than 40 days. Because the lag-time of T_{gH1} to reach 37°C ($t_{lag\ 37°C}$), e.g., to convert the polymer matrix to a rubbery state, nearly coincided with the lag-time (t_i) prior to the onset of the accelerated degradation phase (k_1), it can be concluded that differences in chain mobility resulting from differences in the physical state of the polymer are responsible for the biphasic degradation kinetics of R 202/I microparticles pre-onset of accelerated bulk erosion. The appearance of a second phase transition at 42°C after 60 days most likely indicates a heterogeneous degradation mechanism with two domains in different physical states: probably a shell in the glassy state and a core in a rubbery state due to an internal accumulation of acidic degradation products.

To further elucidate the possible reason for the final slow-down of the degradation rate post-onset of erosion, it was necessary to consider the physical and morphological changes associated with particle erosion. It was interesting to see that particle erosion was associated with an increase in bulk-water content as observed by an increase in the area under the melting peak (T_m) around 0°C (Fig. 3). This result is plausible since bulk erosion causes an increase in matrix porosity, thus allowing the water to penetrate into the particle bulk. Obviously, as indicated by the appearance of a distinct shoulder prior to the main melting peak (T_m) of bulk-water around 0°C at day 105, the porosity increase also allowed the penetration of buffer ions into the polymer bulk. This phenomenon is of particular importance for a correct interpretation of the time-dependent changes in the phase transitions obtained in the DSC thermograms of the dried microparticles pre-onset and post-onset of erosion (Figs. 4a and 4b).

As shown in Fig. 4a and summarized in Table 4, the glass transition temperature (T_{gD}) of the dried R 202/I microparticles remained nearly unchanged during the induction period (t_i) with the usual differences (ΔT) between the first and second run indicating enthalpy relaxation processes. After day 60, a T_g-splitting was observed, thus confirming the DSC results obtained with the hydrated microparticles (Fig. 2) and the conclusion drawn that two different domains with different glass transition temperatures (T_{gD1} and T_{gD2}) have to be distinguished. Interestingly, as evidenced by the DSC traces in Fig. 4b, a sudden drop of the lower T_{gD1} from 42°C at day 75 (pre-onset of erosion) down to −14.8°C at day 90 (post-onset of erosion) with a further shift down to −51.3°C at day 105 could be detected during the first run. At day 105, an additional melting peak around 162°C, resulting from crystallized buffer salts, could be observed. Both transitions intensified as time progressed and equilibrated around −38°C and 165°C, respectively. T_{gD2} remained, however, constant around 50°C, irrespective of the degradation time. In the second run, only a single T_g, shifting to lower temperatures as time progressed, but no melting peaks were observed over the whole time scale.

Fig. 5 illustrates and summarizes the time-dependent changes of the phase transitions determined from the DSC thermograms of the dried microparticles during the first and the second run, and their relation to the kinetic parameters obtained by GPC and gravimetry. From this graph the following findings are evident: First, the first T_g-splitting observed in the first run nearly coincided with the onset (t_i) of the accelerated degradation phase characterized by k_1. Second, the abrupt drop of T_{gD1} occurred shortly after the onset of bulk erosion ($t_{lag\ ML}$),

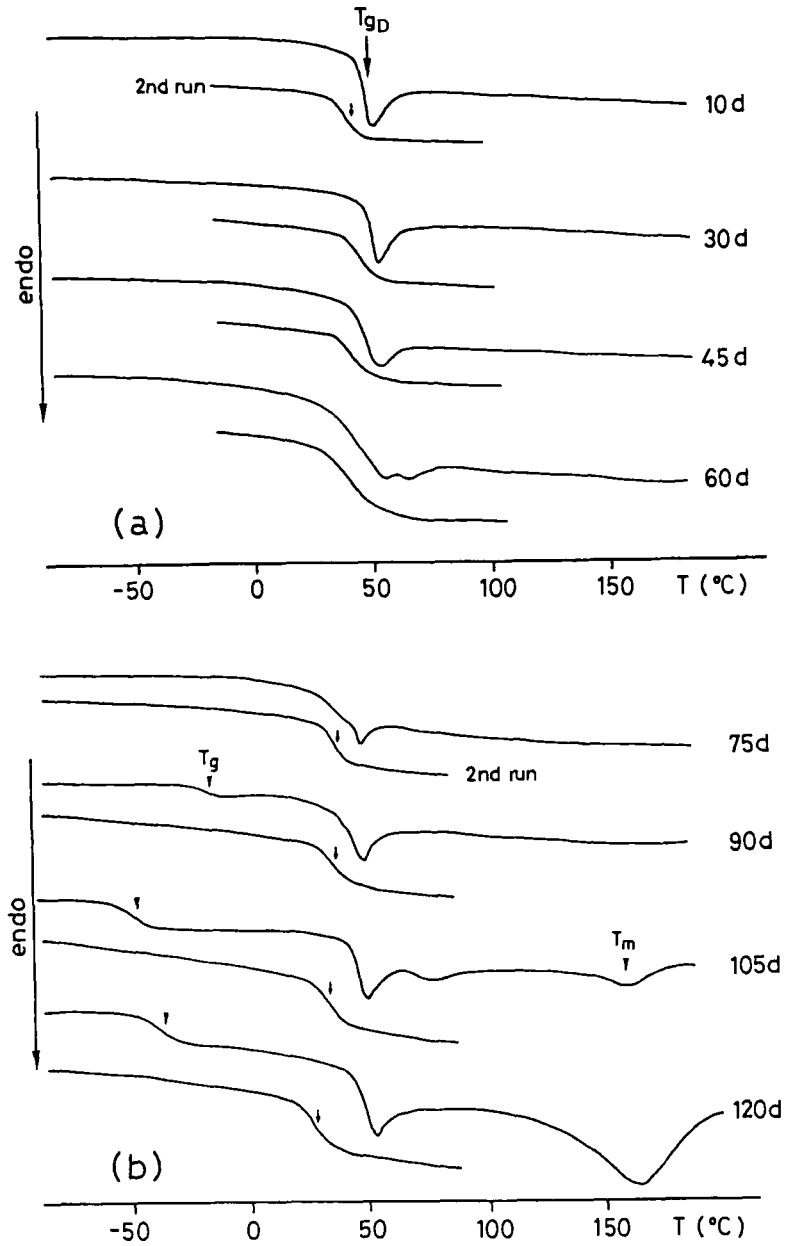

Figure 4. DSC thermograms of dried R 202/I microparticles after various incubation times in 0.1 M PBS pH 7.4 of 37°C: (a) pre-onset of erosion, (b) post-onset of erosion.

which was associated with an increase in bulk-water uptake. Third, this second T_{gD1} drop was significantly intensified post-onset of accelerated penetration of buffer ions into the particle bulk (see also Fig. 3) and clearly related to the onset of the final degradation phase ($t_{lag\ k2}$).

Considering all these findings together with the observation that post-onset of buffer ion penetration into the particle bulk, increasing amounts of the remaining particle mass remained undissolved in tetrahydrofuran (THF) used for GPC measurements, it can be concluded that the T_g-splitting is obviously a buffer-induced phase

Table 4

DSC Data of Dried PLA and PLGA Microparticles During In Vitro Degradation in 0.1 M PBS pH 7.4 of 37°C (n = 3)

	Phase Transitions[a]											
	R 202/I			RG 755/I			RG 755/II			RG 755/III		
t(*d*)	T_{g1} (°C)	T_{m1} (°C)	T_{g2} (°C)	T_{g1} (°C)	T_{m1} (°C)	T_{g2} (°C)	T_{g1} (°C)	T_{m1} (°C)	T_{g2} (°C)	T_{g1} (°C)	T_{m1} (°C)	T_{g2} (°C)
0	49.0		47.4	48.3		47.4	45.1		43.6	48.8		48.0
2	50.1		46.8	49.9		46.4	47.0		44.1	49.9		47.8
10	50.4		46.0	50.8		44.8	–15.3/49.8		38.7	51.0		46.6
20	51.0 48.0		47.1	51.0		45.1	–47.6/46.2	162.4	26.0	52.0		
30	51.5		47.7	48.1		43.8	–45.8/46.3	162.2	25.3	51.8		48.1
45	50.3		44.0	44.8		41.8	–44.5/45.5	160.8	24.0	50.9		45.3
60	44.0/52.0		40.5	43.6		40.1	–41.1/46.2	152.0/166.8	24.8	48.8		44.8
75	42.0/49.5		38.0	–12.0/44.1		33.8				48.0		43.1
90	–14.8/48.1		33.1	–49.9/43.5	156.8	24.6				46.9		34.2
105	–51.3/49.2	162.5	29.9	–45.3/43.8	158.3	20.4				–3.0/46.6		32.1
120	–38.8/50.1	165.4	25.8	–41.0/44.0	155.0	18.0				–5.2/46.0		30.8

[a] T_{g1}: Glass transition temperatures (T_{gD}) of first heating cycle.
[b] T_{m1}: Melting peaks of first heating cycle.
[c] T_{g2}: Glass transition temperatures (T_{gD}) of second heating cycle.

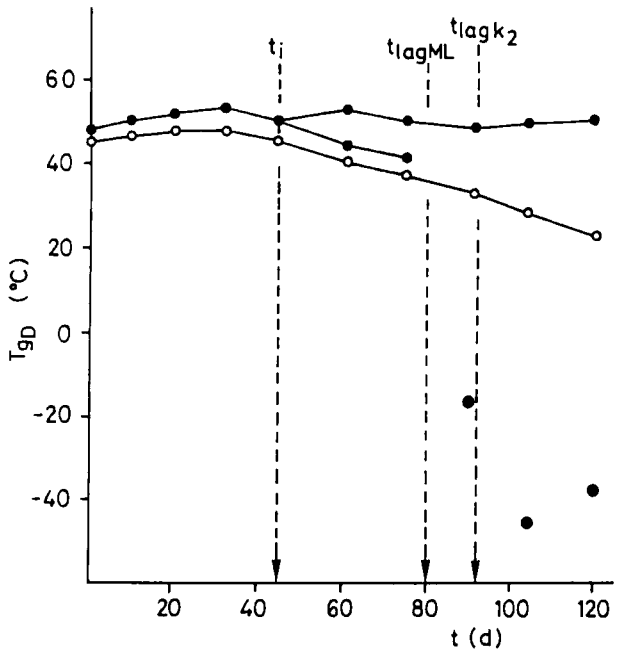

Figure 5. Time-dependent changes in the glass transition temperature (T_{gD}) of dried R 202/I microparticles: (●) first run, (○) second run; $n = 3$.

separation effect. What obviously occurred during particle hydration and degradation was an ionization and sodium salt formation of the acidic degradation products in contact with the buffer solution of pH 7.4, leading to an apparent increase in their water solubility, and thus to their abrupt exclusion as plasticizer and autocatalyst for the water-insoluble polymer matrix. Pre-onset of accelerated bulk erosion, the effect, along with a rapid release of the water-soluble oligo- and monomers, was restricted to the particle surface leading to core and shell domains in different physical states. Post-onset of accelerated bulk erosion, the overall particle bulk was affected, however, without a distinct release of the water-soluble compounds from the core. The final reduction of the overall degradation rate post-onset of bulk erosion is therefore the combined result of a rapid surface release and a certain accumulation of the phase-separated oligo- and monomers within the particle bulk. Confirmation of the proposed mechanisms is provided by the single, gradually decreasing T_{gD} observed in the DSC scans of the second run (Figs. 4b and 5), which clearly indicates the miscibility and plasticizing effect of the phase-separated compounds in the equilibrium state.

Degradation of RG 755 Microparticles

The proposed degradation mechanisms determining the different degradation kinetics of 55 μm R 202/I microparticles were confirmed by the results obtained with RG 755/I microparticles prepared by the same procedure and having approximately the same particle size (see Table 1). In fact, as illustrated in Figs. 6 and 7a, the same triphasic degradation profile associated with qualitatively the same physical and morphological events could be observed with 60 μm RG 755/I microparticles. Only the absolute values of the kinetic and thermal parameters were found to be different (see Tables 2–4) reflecting differences in chemical composition (LA/GA-ratio) and weight average molecular weight. Mechanistic details concerning the effects of polymer composition and weight average molecular weight on the degradation kinetics of PLA/PLGA microspheres and films will be addressed further in a forthcoming paper.

Particle Size Effects

To study particle size effects on the degradation behavior of RG 755 microparticles, the 60 μm sample (RG 755/I) was compared with two samples of approximately 2 μm mean particle size prepared by two different techniques: a modified o/w technique using probe sonication to reduce the particle size (RG 755/II), and a novel flocculation technique based on water-soluble solvents, thus

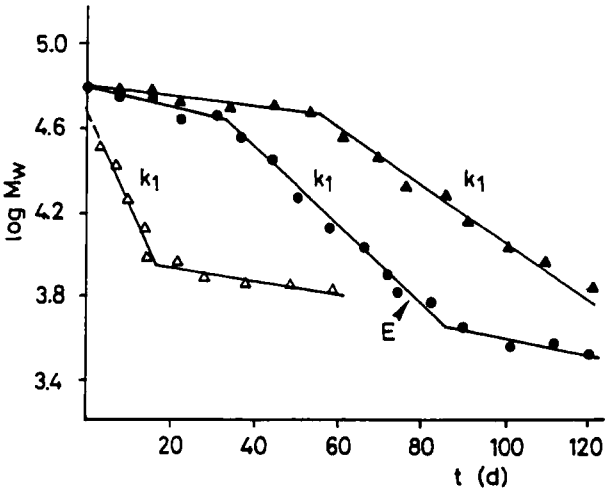

Figure 6. Time-dependent M_W-changes of RG 755 microparticles immersed in 0.1 M PBS pH 7.4 of 37°C: (●) RG 755/I, (Δ) RG 755/II, (▲) RG 755/III; $n = 3$; (for details of I, II, and III see Table 1).

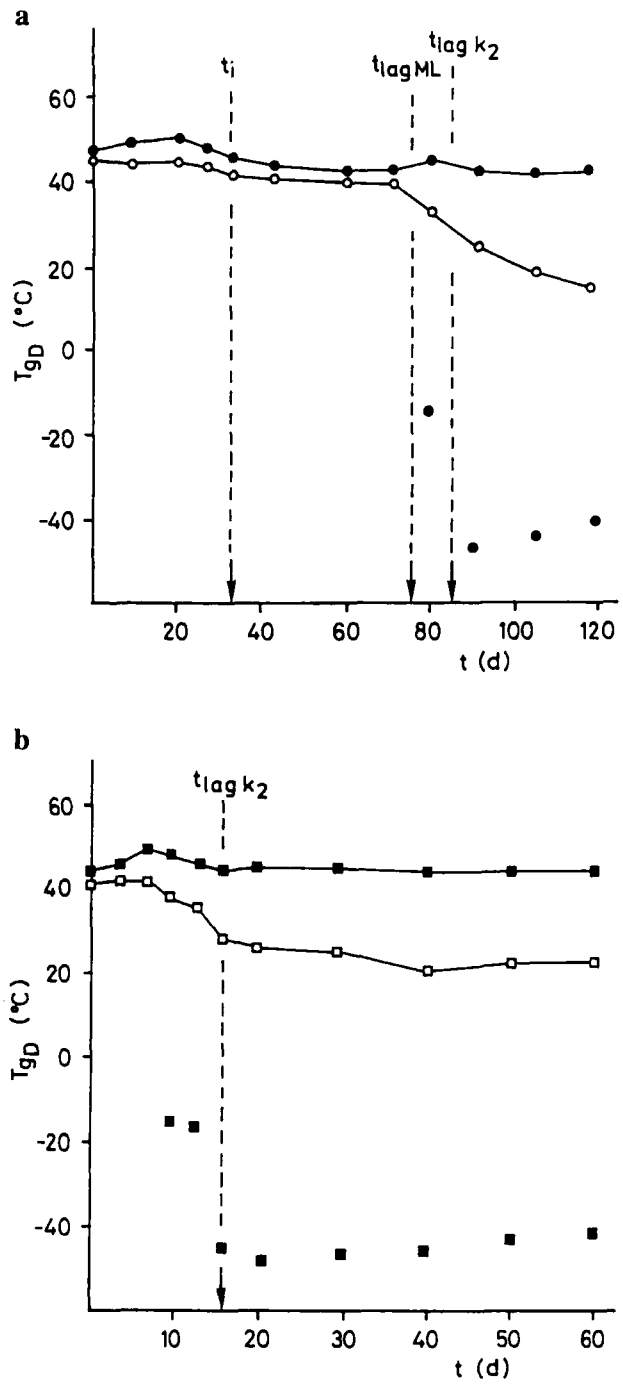

Figure 7. Time-dependent changes in the glass transition temperature (T_{gD}) of dried (a) RG 755/I, (b) RG 755/II, and (c) RG 755/III microparticles; (●, ■, ▲) first run, (○, □, Δ) second run; n = 3.

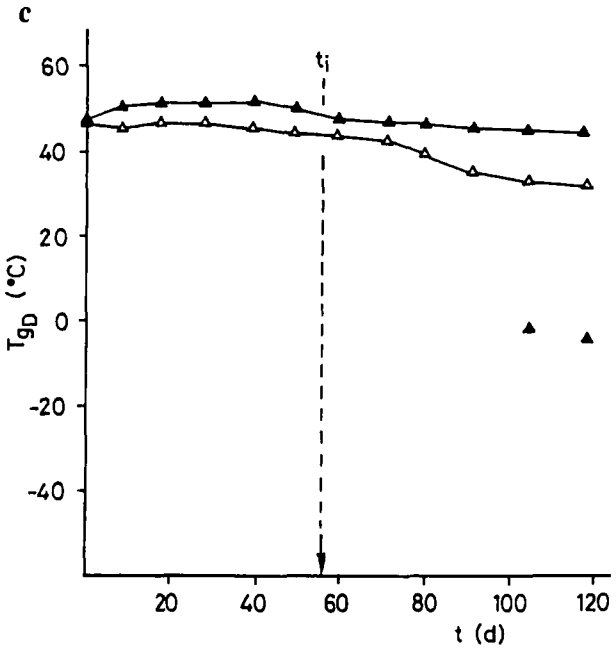

Figure 7. Continued

avoiding highly energetic homogenization techniques (RG 755/III).

The RG 755/II and RG 755/III microparticles had a mean particle size of 2.5 μm and 1.8 μm, respectively. Particle size distribution was relatively small in both cases with 95% of the particles having a diameter of less than 10 μm, thus indicating statistically significant differences compared to RG 755/I particles with respect not only to mean particle size, but also to the particle size distribution. As indicated in Table 1, probe sonication (II) was found to significantly affect the particle characteristics in such a way as to induce a substantial decrease in M_w from 66.8 kDa (polymer raw material) to 46.5 kDa (RG 755/II microparticles), and a tremendous increase in polydispersity (PD) from 1.7 (polymer raw material) to 8.2 (RG 755/II microparticles). Polymer characteristics of RG 755/III microparticles prepared without probe sonication remained, however, unchanged during microparticle processing.

Irrespective of the preparation technique, the log M_w versus time profiles of both 2 μm samples (II and III) were biphasic over the time scale studied (Fig. 6) and thus, different from the triphasic degradation profile observed with the 60 μm particles (I). Significant dif-

ferences in the degradation rates within the two distinct kinetic phases were, however, observed between sample II and sample III. Comparing the first-order rate constants of the different degradation phases (see Table 2), it seemed reasonable to assume that degradation of sample II started directly in the accelerated phase (k_1) with a significantly faster degradation rate than sample I and III during this phase. The lag-time ($t_{lag\ k2}$) prior to the onset of the final slow degradation phase (k_2) was only 16 days, suggesting a fast onset of bulk erosion due to the initial presence of a high amount of low molecular weight degradation products. In fact, the GPC traces changed rapidly from bimodal to monomodal, suggesting either a fast release or a fast phase separation of the low molecular weight degradation products.

The degradation profile of sample III (Fig. 6) suggested an induction period (t_i) of 56 days followed by the accelerated degradation phase with a slightly lower k_i than sample I and a much lower k_i than sample II. A final slow-down could not, however, be observed over the time scale studied.

The kinetic differences observed between sample I and sample III were supposed to result exclusively from particle size differences. Kinetic differences between the samples I and II or II and III were likely to be mainly induced or further affected by differences in the molecular weight distribution of the polymer.

To confirm these suggestions and to elucidate the relative importance of particle size and molecular weight distribution for the observed degradation kinetics, hydrated and dried RG 755/II and RG 755/III microparticles were subjected to a DSC study and the data compared to those obtained for RG 755/I microparticles. The results are summarized in Tables 3 and 4 and illustrated in Figs. 6–10.

Samples varying in particle size and/or molecular weight distribution showed significant differences in their glass transition temperature (T_{gH}) after 2 days of incubation (Fig. 8) and in their $t_{lag\ 37°C}$ (Fig. 9). RG 755/I and RG 755/III microparticles of comparable polymer characteristics, but different particle size, both remained in a glassy state for 33 and 57 days, respectively. The glassy state clearly explains the induction period observed in both samples, irrespective of their particle size. The differences in the absolute values of T_{gH} during this period and in $t_{lag\ 37°C}$, e.g., in the duration of the induction period (t_i), most likely reflect differences in particle size. As summarized in Table 4

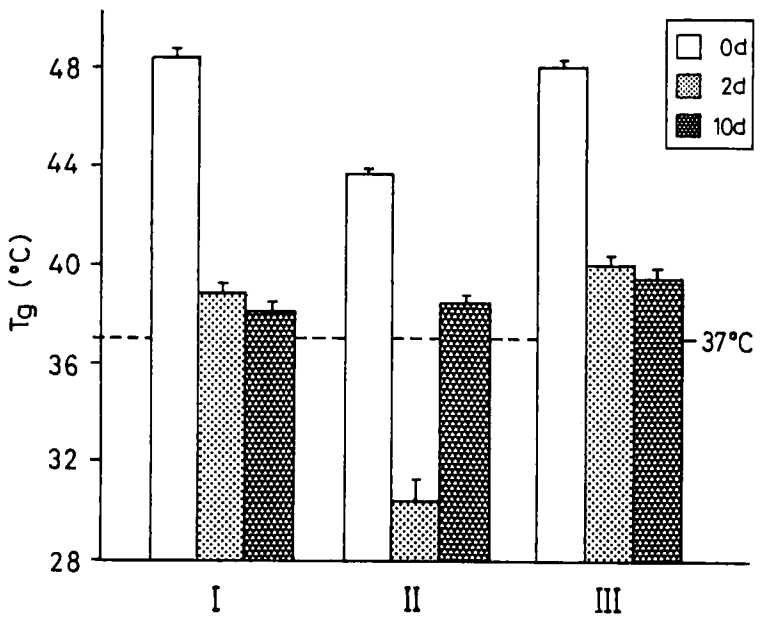

Figure 8. Effect of particle size (I, III) and preparation technique (II, III) on the glass transition temperature (T_{gH}) of hydrated RG 755 microparticles after 0 days, 2 days, 10 days in 0.1 M PBS pH 7.4 of 37°C; $n = 3$.

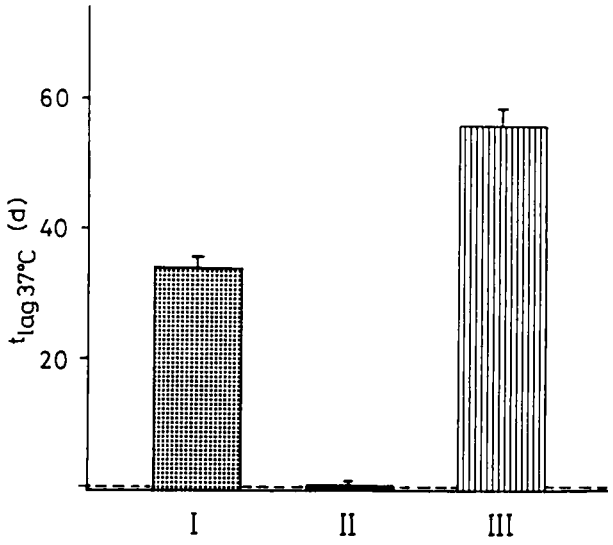

Figure 9. Effect of particle size (I, III) and preparation technique (II, III) on the lag-time of $T_{gH} < 37°C$ of RG 755 microparticles ($n = 4$; for details of I, II and III see Table 1).

and illustrated in Figs. 7a and 7c, the glass transition temperatures (T_{gD}) of the dried samples, calculated from the first and second run, were significantly higher for the 2 μm particles (III) than for the 60 μm particles (I) over the entire time scale of 120 days. Moreover, the appearance of a second T_g in the low-temperature range during the first run, indicating the buffer-induced phase separation of oligomers within the particle bulk was less pronounced in sample III and could only be observed after day 105. These findings clearly suggest that phase separation phenomena within the particle bulk are less pronounced. It is therefore evident that the higher surface-to-volume ratio of 2 μm particles compared to 60 μm particles allowed a faster and more continuous release of water-soluble degradation products from the smaller particles, thus leading to a overall slower degradation rate with no such distinct kinetic differences pre-onset and post-onset of bulk erosion as observed with 60 μm particles.

RG 755/II microparticles, the molecular weight distribution of which was strongly affected by the preparation procedure (see Table 1), showed an immediate T_g-shift from 43.6°C down to 30.4°C within the first hours of incubation (Fig. 8). The initial presence of a high amount of low molecular weight oligomers produced by probe sonication obviously allowed the hydrated particle morphology to immediately convert from a glassy to a rubbery state. The high chain mobility of all polymer molecules resulting from one single $T_{gH/1d}$ well below 37°C and the additional autocatalytic effect of the initially present acidic degradation products being homogeneously mixed with the high molecular weight polymer fraction clearly explains the high initial degradation rate, e.g., the immediate onset of the accelerated degradation phase with a significantly higher k_1 than sample I and III (see Table 2).

The short duration of the accelerated degradation phase, which was reflected by the short $t_{lag\ k2}$ of 16 days, turned out to be the result of a combination of two opposing processes associated with the porosity increase due to the rapid onset of bulk erosion and resulting in a complete loss of the initially present oligomers as plasticizer and catalyst. These two opposing processes were

- diffusion of water-soluble oligomers *out* of the particle bulk and
- penetration of bulk-water and buffer ions *into* the particle bulk.

The proposed mechanism is clearly indicated by several pieces of evidence obtained from the DSC thermograms of the hydrated and dried RG 755/II samples. First, the glass transition temperature (T_{gH}) rapidly increased from 30.4°C at day 2 up to 38.4°C at day 10 (Fig. 8 and Table 3) indicating a change from the rubbery to a glassy state. Second, the DSC thermograms of the hydrated RG 755/II microparticles showed increasing bulk-water melting peaks around 0°C after 2 days of incubation, with a distinct shoulder prior to the main peak at day 20 and a pronounced overall T_m-peak shift below 0°C at day 60 (Fig. 10) indicating penetration of buffer ions into the particle bulk. Finally, the rapid appearance of two distinct phase transitions (T_{gD1} and T_{gD2}) in the first DSC scan of the dried microparticles after day 10, corresponding to water-soluble oligomers and water-insoluble polymer molecules in different phases and physical states, their nearly constant values over the entire time scale, their temperature-induced miscibility resulting in a single intermediate, and nearly constant T_{gD} in the second run (Fig. 7b and Table 4), clearly reveal a rapid phase separation of part of the initially present oligomers to occur within the particle bulk.

CONCLUSIONS

The study revealed that DSC is a useful analytical technique to study the morphological and physical changes of PLA and PLGA microparticles during their

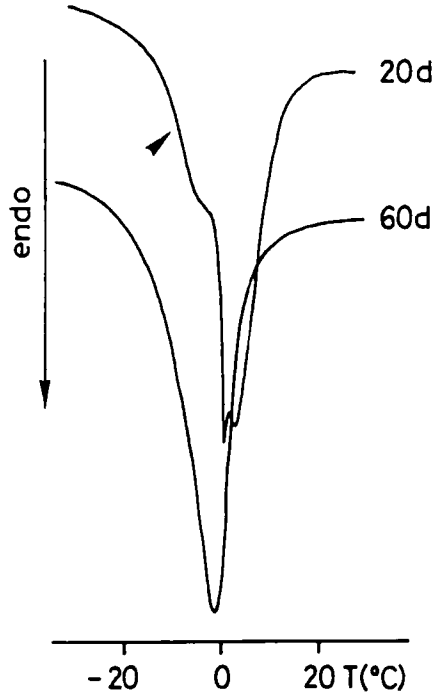

Figure 10. Melting endotherms of water within hydrated RG 755/II microparticles after 20 days and 60 days in 0.1 M PBS pH 7.4 of 37°C.

hydration and degradation. Important parameters such as phase separation phenomena, the physical state of the absorbed water, and the penetration of buffer ions into the particle bulk can be monitored, thus elucidating the mechanisms underlying the bi- or triphasic degradation profiles of PLA and PLGA microparticles. The most striking findings of the present DSC studies are

- Evidence for the glass transition temperature (T_{gH}) of the hydrated particles to be the most critical parameter determining the degradation kinetics pre-onset of accelerated bulk erosion.
- A mechanistic explanation for the observed decrease in the degradation rate post-onset of bulk erosion, namely a permeability increase of the particle bulk for buffer ions leading to a salt formation and subsequent phase separation of the water-soluble degradation products, thus reducing their plasticizing and autocatalytic contribution to the overall degradation rate.
- Particle size effects on the degradation kinetics are by no means straightforward, since preparation-induced degradation phenomena affecting the aforementioned parameters have to be considered.

Current studies focus on drug and excipient effects and the role of buffer species and concentration in the degradation behavior of PLA and PLGA microparticles. Results from these studies will be presented in several forthcoming papers.

REFERENCES

1. F. G. Hutchinson and B. J. A. Furr, J. Contr. Rel., 13, 279 (1990).
2. F. G. Hutchinson, Eur. Patent 0058481 (1986).
3. X. Zhang, U. P. Wyss, D. Pichora, and M. F. A. Goosen, J. Contr. Res., 31, 129 (1994).
4. Y. Ogawa, H. Okada, M. Yamamoto, and T. Shimamoto, Chem. Pharm. Bull., 36, 2576 (1988).
5. S. Cohen, T. Yoshioka, M. Lucarelli, L. H. Hwang, and R. Langer, Pharm. Res., 8, 713 (1991).
6. M. J. Alonso, S. Cohen, T. G. Park, R. K. Gupta, G. R. Siber, and R. Langer, Pharm. Res., 10, 945 (1993).
7. J. H. Eldridge, J. K. Staas, J. A. Meulbroek, J. R. McGhee, T. R. Tice, and R. M. Gilley, Mol. Immunol., 28, 287 (1991).
8. S. M. Li, H. Garreau, and M. Vert, J. Mater. Sci. Mater. Med., 1, 123 (1990).
9. S. M. Li, H. Garreau, and M. Vert, J. Mater. Sci. Mater. Med., 1, 131 (1990).
10. S. M. Li, H. Garreau, and M. Vert, J. Mater. Sci. Mater. Med., 1, 198 (1990).
11. M. Vert, S. Li, and H. Garreau, J. Contr. Rel., 16, 15 (1991).
12. M. Herrlinger, Dissertation, Heidelberg, 1994.
13. M. Iwata and J. W. McGinity, Pharm. Res., 10, 1219 (1993).
14. G. E. Visscher, R. L. Robison, H. V. Maulding, J. W. Fong, J. E. Pearson, and G. J. Argentieri, J. Biomed. Mater. Res., 19, 349 (1985).
15. G. E. Visscher, R. L. Robison, H. V. Maulding, J. W. Fong, J. E. Pearson, and G. J. Argentieri, J. Biomed. Mater. Res., 20, 667 (1986).
16. I. Grizzi, S. Garreau, S. Li, and M Vert, Biomaterials, 16, 305 (1995).
17. A. G. Hausberger, R. A. Kenley, and P. A. DeLuca, Pharm. Res., 12, 851 (1995).
18. C. Thomasin, G. Corradin, Y. Men, H. P. Merkle, and B. Gander, J. Contr. Rel. 41, 131 (1996).
19. T. Heya, H. Okada, Y. Ogawa, and H. Toguchi, J. Pharm. Sci., 83, 636 (1994).
20. G. Reich, Eur. J. Pharm. Biopharm. (accepted).
21. T. G. Park, J. Contr. Rel., 30, 161 (1994).